A study on the energy transfer of a square prism under fluid-elastic galloping

H.G.K.G. Jayatunga, B.T. Tan, J. S. Leontini

Abstract

Extracting useful energy from flow induced vibrations has become a developing area of research in recent years. In this paper, we analyse power transfer of an elastically mounted body under the influence of aeroelastic galloping. The system and the power transfer is analysed by numerically integrating the quasi-steady state model equations. The power transfer is analysed for both high ($Re = 22300$) and low ($Re = 165$) Reynolds numbers cases, and the impact of the system mass is investigated for both.

At high mass ratios ($m^* > 50$), the power transfer is completely controlled by galloping and essentially independent of the mass. A combined mass-damping coefficient, Π_2, that can be derived from the equation of motion, is shown to be the parameter that governs power output. The system is a balance between the power delivered to the system due to hydrodynamic forcing and power removed through mechanical damping which are governed by the hydrodynamic forcing characteristics (i.e. the lift force as a function of incident angle) and mechanical damping coefficient respectively. The peak efficiency of 0.26% for $Re = 165$ and 6.7% for $Re = 22300$ were observed when the non-dimensionalised mass-damping factor becomes 0.314 and 1.04 respectively.

A contradictory behaviour is observed at low m^* between the low and high Re cases. The forcing due to vortex shedding at low Reynolds numbers suppresses the galloping excitation and results in a reduced power output. For the case with high Re power output increases as m^* is reduced . For this high Re case, at low m^* the reduction in inertia allows the body to accelerate faster and spend a larger portion of the period at relatively high transverse velocities. Extrapolating this trend, the limit to peak efficiency is found to be 13.5% and occurs when $m^* \to 0$ and $U^* \to \infty$ and $\Pi_2 = 1.22$

Keywords:

1. Introduction

Fluid-elastic galloping is one of the sub-areas of research in fluid structure interactions. This area has been of interest due to the vibrations crated by galloping on transmission lines and civil structures and leading them to failure. Therefore understanding this phenomenon in order to suppresses these vibrations was quite important. However, the search for alternate energy sources with minimal environmental impact has become an important area of research in the modern word. Therefore researchers are moving towards investigating

the possibility of extracting useful energy from this vibrations rather than suppressing them. Thus, it is quite important to understand the governing parameters and analyse the influence of them on the energy transfer from the fluid to the structure, because this understanding will lead to develop better practical applications. Hence, in this paper we focus on understanding the energy transfer from the fluid to the body and isolate the governing parameters influencing it.

According to Païdoussis et al. (2010), Glauert (1919) provided a criterion for galloping by considering the auto-rotation of an aerofoil. Den Hartog (1956) provided a theoretical explanation for galloping for iced electric transmission lines. A weakly non-linear theoretical aeroelastic model to predict the response of galloping was developed by Parkinson and Smith (1964) based on the quasi-steady state hypothesis. Experimental lift and drag data on a fixed square prism at different angles of attack were used as an input for the theoretical model. It essentially used a curve fit of the transverse force to predict the galloping response. The study managed to achieve a good agreement with experimental data.

However, the QSS model equation when solved analytically using the sinusoidal solution method cannot predict the response for cases with low mass ratios. Joly et al. (2012) observed that finite element simulations show a sudden change in amplitude below a critical value of the mass ratio. The quasi-oscillator equation in Parkinson and Smith (1964) was altered to account for the vortex shedding and solved numerically to predict the reduced amplitude at low mass ratios to the point where galloping is no longer present. Barrero-Gil et al. (2010) investigated the possibility of extracting power from vibrations caused by galloping using the quasi-steady state model. In the conclusions of that paper it was pointed out that in order to obtain a high power to area ratio, the mass-damping $(m^*\zeta)$ parameter should be kept low. The same study investigated the influence of the characteristics of the C_y curve on maximum power output.

Here, the modified QSS model developed by Joly et al. (2012) is integrated numerically for low Reynolds numbers. The focus is on the power transfer from the fluid to the structure and the influence of mechanical parameters (i.e. frequency of oscillation, damping factor and mass ratio). To this end, a series of previously mentioned mechanical parameters are tested at two different values of Re: $Re = 165$, a case that should remain laminar and essentially two-dimensional; $Re = 22300$, a case where the flow is expected to be turbulent and three-dimensional. Both cases require the input of transverse force coefficients C_y as a function of angle of attack θ for a fixed body. These data are provided from direct numerical simulations for the $Re = 165$ case, while the data provided by Parkinson and Smith (1964) are used for the $Re = 22300$ case.

The structure of the paper is as follows. Section 2 presents the governing equations and the oscillator model used to obtain data, the method for the calculation of the power transferred from the fluid to the structure. The governing parameters namely, the combined mass-stiffness and the combined mass-damping obtained using linearised time scales of the oscillator model are also being introduced. Section 3 presents the results, first of the fixed body tests at a range of θ, then of the response characteristics predicted by the integration of the QSS model for both the high and low Re cases. For the low Re case, the results of the QSS model are compared to those of full direct numerical simulations of the fluid-structure

interaction problem. Finally, section 4 presents the conclusions that can be drawn from this work.

Nomenclature

|	
a_1, a_3, a_5, a_7	coefficients of the polynomial to determine C_y
A	displacement amplitude
c	damping constant
D	characteristic length (side length) of the cross section of the body
$f = \sqrt{k/m}/2\pi$	natural frequency of the system
F_y	instantaneous force normal to the flow
F_0	amplitude of the oscillatory force due to vortex shedding
k	spring constant
m	mass of the body
m_a	added mass
P_d	power dissipated due to mechanical damping
$P_{in} = \rho U^3 D/2$	Energy flux of the approaching flow
P_{mean}	mean power
P_t	power transferred to the body by the fluid
t	time
U	freestream velocity
U_i	Induced velocity
$y, \dot{y}, \ddot{y}$	transverse displacement, velocity and acceleration of the body
$\mathcal{A} = DL$	frontal area of the body
λ	Inverse time scale of a galloping dominated flow
$\lambda_{1,2}$	Eigenvalues of linearized equation of motion
ρ	fluid density
$\omega_n = 2\pi f$	natural angular frequency of the system
ω_s	vortex shedding angular frequency
$c^* = cD/mU$	non-dimensionalised damping factor
$C_y = F_y/0.5\rho U^2 DL$	normal (lift) force coefficient
$m^* = m/\rho D^2 L$	mass ratio
Re	Reynolds number
$U^* = U/fD$	reduced velocity
$Y = y/D$	non-dimensional transverse displacement
$\dot{Y} = m^*\dot{y}/a_1 U$	non-dimensional transverse velocity
$\ddot{Y} = m^{*2}D/a_1^2 U^2$	non-dimensional transverse acceleration
$\Gamma_1 = 4\pi^2 m^{*2}/U^{*2}a_1^2$	First dimensionless group arising from linearised, non-dimensionalised equation
$\Gamma_2 = c^* m^*/a_1$	Second dimensionless group arising from linearised, non-dimensionalised equati
$\zeta = c/2m\omega_n$	damping ratio
$\theta = \tan^{-1}(\dot{y}/U)$	instantaneous angle of incidence (angle of attack)
$\Pi_1 = 4\pi^2 m^{*2}/U^{*2}$	Combined mass-stiffness parameter
$\Pi_2 = c^* m^*$	Combined mass-damping parameter
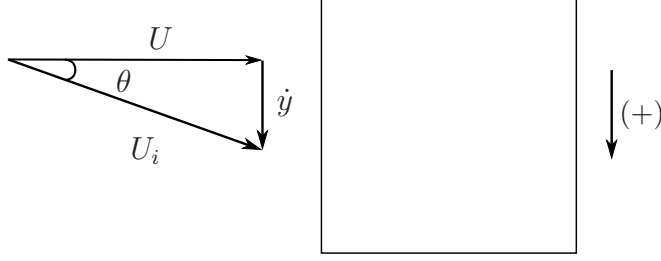
Figure 1: Induced angle of attack on the square prism due to the resultant of free-stream velocity of the fluid and transverse velocity of the body.

2. Problem formulation and methodology

2.1. The quasi-steady state (QSS) model

The equation of motion of the body is given by

$$(m + m_a)\ddot{y} + c\dot{y} + ky = F_y, \tag{1}$$

where the forcing term F_y is given by

$$F_y = \frac{1}{2}\rho U^2 \mathcal{A} C_y. \tag{2}$$

Lighthill (1986) showed that for systems oscillating in fluid, it is sometimes useful to decompose the fluid forces into components that are in and out of phase with the body acceleration. The component in phase with the acceleration effectively adds to the inertia or effective mass of the system. Therefore, an added mass term, m_a, can be added to the system mass. For consistency with previous studies such as Joly et al. (2012), a value of $m_a = 3.5$ has been used here.

In the QSS model, it is assumed that the force on the body at a given instantaneous incident angle θ (defined in figure 1) is the same as the mean force on a static body at the same incident angle, or angle of attack. The instantaneous value of C_y is therefore determined by an interpolating polynomial based on the lift data for flow over a stationary body at various θ. Using the relationship between θ and the instantaneous transverse velocity of the body $\dot{y}$ shown in figure 1, C_y can be written as a function of $\dot{y}$. The order of the interpolation polynomial used to define this function has varied from study to study. For example a 7th order polynomial was used in Parkinson and Smith (1964) and 3rd order polynomial was used in Barrero-Gil et al. (2009). Ng et al. (2005) concluded that using a 7th order polynomial is sufficient and a polynomial higher than that of 7th order doesn't provides a significantly better result. Thus a 7th order interpolating polynomial is used in this present study. As a result, $C_y(\theta)$ (noting that theta is proportional to $\dot{y}/U$) is defined as

$$C_y(\theta) = a_1 \left(\frac{\dot{y}}{U}\right) + a_3 \left(\frac{\dot{y}}{U}\right)^3 + a_5 \left(\frac{\dot{y}}{U}\right)^5 + a_7 \left(\frac{\dot{y}}{U}\right)^7. \tag{3}$$

It is expected that vortex shedding will be well correlated along the span and provide significant forcing at low Re. Joly et al. (2012) introduced an additional sinusoidal forcing function to the hydrodynamic forcing to model this. This enables the model to provide accurate predictions even at low mass ratios where galloping excitation is suppressed or not present. In this study, the forcing due to vortex shedding in low Re cases is incorporated using a sinusoidal forcing function $F_0 \sin \omega_s t$ added to the right-hand side of equation 1. Here, ω_s and F_0 represent the angular vortex shedding frequency and the maximum force due to shedding respectively. Thus, the final equation for the modified QSS model is

$$m\ddot{y}+c\dot{y}+ky=\frac{1}{2}\rho U^2 \mathcal{A}\left(a_1\left(\frac{\dot{y}}{U}\right)+a_3\left(\frac{\dot{y}}{U}\right)^3+a_5\left(\frac{\dot{y}}{U}\right)^5+a_7\left(\frac{\dot{y}}{U}\right)^7\right)+F_0\sin\left(\omega_s t\right). \tag{4}$$

This equation can be solved using standard time integration methods. In this study the fourth-order Runge-Kutta scheme built in to the MATLAB routine 'ode45' was generally used to obtain the solutions. Some low mass ratio cases used a solver modified for stiff problems, built into the 'ode15s' routine in MATLAB.

2.2. Calculation of average power

The dissipated power due to the mechanical damping represents the ideal potential amount of harvested power output. Therefore, the mean power output can be given by

$$P_{mean} = \frac{1}{T}\int_0^T (c\dot{y})\dot{y}dt, \tag{5}$$

where T is the period of integration and c is the mechanical damping constant.

It should be noted that this quantity is equal to the work done on the body by the fluid, defined as

$$P_{mean} = \frac{1}{T}\int_0^T F_y\dot{y}dt, \tag{6}$$

where F_y is the transverse (lift) force.

These two definitions show two important interpretions of the power with respect to any energy production device. The first shows that power will be high for situations where the damping coefficient is high, and the transverse velocity is consistently high. The second shows that power will be high for situations where the transverse force and the body velocity are in phase.

The natural time scales of the system can be found by solving for the eigenvalues of the linearized equation of motion, namely

$$(m + m_a)\ddot{y}+c\dot{y}+ky=\frac{1}{2}\rho U^2 \mathcal{A}a_1\left(\frac{\dot{y}}{U}\right), \tag{7}$$

which is simply the equation of motion presented in equation 4 with the polynomial series for the lift force truncated at the linear term, and the forcing term representing vortex shedding removed.
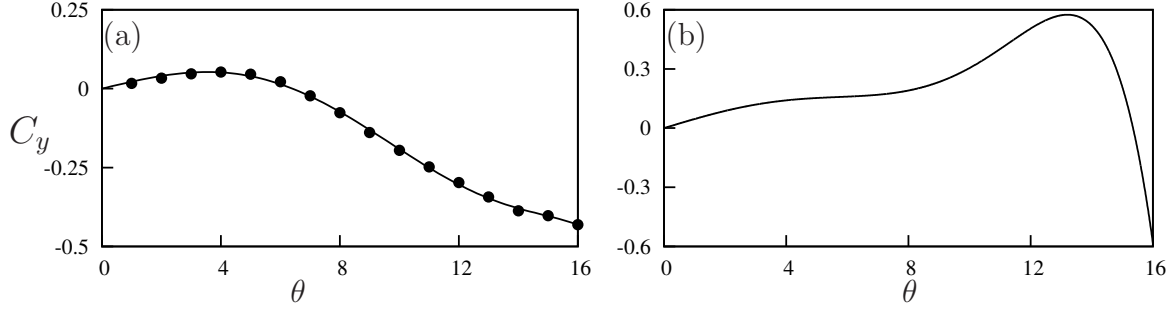
Figure 2: Lift coefficient, C_y, as a function of incidence angle θ, for a static square cross section. (a) Data from simulations at $Re = 165$ (b) data from Parkinson and Smith (1964) at $Re = 22300$. Points (•) are measurements from the simulations. The solid lines in both plots are 7th-order interpolating polynomial used to predict the fluid forcing for the QSS model. C_y is the force coefficient of the force which occurs normal to the induced velocity.

Case	a_1	a_3	a_5	a_7
Re=165	1.3	125.3	1825.73	8765.3
Re=22300	2.69	168	1670	59900

Table 1: Coefficient values used in the 7th order interpolation polynomial for high ($Re = 22300$) and low ($Re = 165$) Reynolds numbers. These data are used as input data to calculate the right-hand side of Eq. 4 throughout this study.

Combining the $\dot{y}$ terms and solving for eigenvalues gives

$$\lambda_{1,2} = -\frac{1}{2}\frac{c - \frac{1}{2}\rho U \mathcal{A} a_1}{(m + m_a)} \pm \frac{1}{2}\sqrt{\left[\frac{c - \frac{1}{2}\rho U \mathcal{A} a_1}{(m + m_a)}\right]^2 - 4\frac{k}{(m + m_a)}}. \tag{8}$$

If it is assumed that the spring is relatively weak, $k \to 0$, a single non-zero eigenvalue remains. This eigenvalue is

$$\lambda = -\frac{c - \frac{1}{2}\rho U \mathcal{A} a_1}{(m + m_a)}. \tag{9}$$

Further, if it is assumed that the mechanical damping is significantly weaker than the aerodynamic forces on the body, $c \to 0$ and

$$\lambda = \frac{\frac{1}{2}\rho U \mathcal{A} a_1}{(m + m_a)}. \tag{10}$$

For reasonably heavy bodies, the impact of the added mass can also be neglected, to arrive at a definition of λ as

$$\lambda = \frac{\frac{1}{2}\rho U \mathcal{A} a_1}{m}. \tag{11}$$

6

In this form, λ represents the inverse time scale of the motion of the body due to the negative damping effect of the long-time aerodynamic forces. In fact, the terms can be regrouped and λ written as

$$\lambda = \frac{a_1}{m^*}\frac{U}{D} \tag{12}$$

Written this way, the important parameters that dictate this inverse time scale are clear. The rate of change in the aerodynamic force with respect to angle of attack when the body is at the equilibrium position, $\partial C_y/\partial \alpha$, is represented by a_1. The mass ratio is represented by m^*. The inverse advective time scale of the incoming flow is represented by the ratio U/D. Increasing a_1 would mean the force on the body would increase more rapidly with small changes in the angle of attack, θ, or transverse velocity. Equation 20 shows that such a change will increase the inverse time scale, or analogously decrease the response time of the body. Increasing the mass of the body, thereby increasing m^*, has the opposite effect. The inverse time scale is decreased, or as might be expected, a heavier body will take longer to respond.

This timescale can then be used to non-dimensionalize the equation of motion, and to find the relevant dimensionless groups of the problem. If the non-dimensional time, τ, is defined such that $\tau = t(a_1/m^*)(U/D)$, the equation of motion presented in equation 4 can be non-dimensionalized as

$$\ddot{Y} + \frac{m^{*2}}{a_1^2}\frac{kD^2}{mU^2}Y = \left(\frac{1}{2} - \frac{m^*}{a_1}\frac{cD}{mU}\right)\dot{Y} + H.O.T., \tag{13}$$

where $H.O.T.$ respresents the higher order terms in $\dot{Y}$. The coefficients can be regrouped into combinations of non-dimensional groups, and rewritten as

$$\ddot{Y} + \frac{4\pi^2 m^{*2}}{U^{*2}a_1^2}Y = \left(\frac{1}{2} - \frac{c^* m^*}{a_1}\right)\dot{Y} + H.O.T, \tag{14}$$

where $c^* = cD/mU$ is a non-dimensional damping parameter.

Equation 22 shows there are four non-dimensional parameters that play a role in setting the response of the system. These are the stiffness (represented by the reduced velocity U^*), the damping c^*, the mass ratio m^*, and the geometry, represented by the rate of change in the aerodynamic force with respect to angle of attack when the body is at the equilibrium position, a_1. The grouping of these parameters into two groups in equation 22 which arise by non-dimensionalising using the natural time scale of the galloping system, suggests there are two groups that dictate the response: $\Gamma_1 = 4\pi^2 m^{*2}/U^{*2}a_1^2$ and $\Gamma_2 = c^* m^*/a_1$. For a given geometry and Reynolds number, Γ_1 can be thought of as a combined mass-stiffness, whereas Γ_2 can be thought of a a combined mass-damping parameter. As it is assumed that during galloping the stiffnes plays only a minor role, Γ_2 seems a likely parameter to collapse the data presented in figure 3. In fact, in the classic paper on galloping from Parkinson and Smith (1964), galloping data from wind tunnel tests is presented in terms of a parameter that can be shown to be the same as Γ_2.

All of the quantities that make up Γ_1 and Γ_2 can, in theory, be known before an experiment is conducted. However, the quantity a_1 is a relatively difficult one to determine, requiring static body experiments or simulations. Here, the geometry is unchanged and results are only being compared at the same Re. Hence, suitable parameters can be formed by multiplying Γ_1 and Γ_2 by a_1^2 and a_1 respectively, to arrive at a mass-stiffness parameter $\Pi_1 = 4\pi^2 m^{*2}/U^{*2}$, and a mass-damping parameter defined as $\Pi_2 = c^* m^*$.

2.3. Parameters used

For the low Re tests, $Re = 165$ was maintained as it was pointed out by Sheard et al. (2009) and Tong et al. (2008) that the three-dimensional transition for a square cylinder occurs at approximately Re=160. F_0 was kept at 0.4937 which was obtained by scaling the value used by Joly et al. (2012) with the amplitude ratios of the lift forces obtained at the different Reynolds numbers.

The angular vortex shedding frequency ω_s, was set to 0.98 which was obtained by performing a power spectral analysis of the stationary data at 0°. Stationary C_y data were obtained at different angles of attack ranging from 0° to 16°. The average power was obtained by using equation 5, and the averaging was done over no less than 20 galloping periods. Predictions of power output at $Re = 22300$ were obtained using the coefficients for curve fitting C_y (Table (1)) from Parkinson and Smith (1964), in order to provide a comparison between high and low Reynolds numbers. The mass ratio m^* was kept at 1163 for $Re = 22300$ (Similar to Parkinson and Smith (1964)) and $m^* = 20$ for Re=165. These parameters were used throughout this study unless otherwise specified.

The stationary data and the fluid-structure interaction (FSI) data were obtained using a high-order spectral element routine to simulate the two-dimensional laminar flow. Simulations involving fluid structure interaction (FSI) were used to provide additional validation of the QSS model. The inlet was placed $20D$ while the outlet situated $60D$ away from the centroid of the body. The side boundaries were placed $20D$ away from the centroid of the body where D was kept as unity throughout this study. The Navier–Stokes equations were solved in an accelerated frame of reference attached to the moving body along with the body equation of motion given in equation 1. A three-step time splitting scheme together with high-order Lagrangian polynomials were used to obtain the solution. The details of the method can be found in Thompson et al. (2006, 1996). This code has been very well validated in a variety of fluid-structure interaction problems (Leontini et al., 2007; Griffith et al., 2011; Leontini et al., 2011; Leontini and Thompson, 2013).

The computational domain consists of 690 quadrilateral macro elements where the majority of the elements were concentrated near the square section. A freestream condition was given to the inlet, top and bottom boundaries and the normal velocity gradient was set to zero at the outlet. A convergence study was performed by changing the order of the polynomial (p-refinement) at $U^* = 40$ and $Re = 165$. A 9th order polynomial together with a time step of $\Delta t U/D = 0.001$ was sufficient to ensure an accuracy of 2% with regards to amplitude of oscillation.

Barrero-Gil, A., Alonso, G., Sanz-Andres, A., Jul. 2010. Energy harvesting from transverse galloping. Journal of Sound and Vibration 329 (14), 2873–2883.

Barrero-Gil, A., Sanz-Andrés, A., Roura, M., Oct. 2009. Transverse galloping at low Reynolds numbers. Journal of Fluids and Structures 25 (7), 1236–1242.

Den Hartog, J. P., 1956. Mechanical Vibrations. Dover Books on Engineering. Dover Publications.

Glauert, H., 1919. The rotation of an aerofoil about a fixed axis. Tech. rep., Advisory Committee on Aeronautics R and M 595. HMSO, London.

Griffith, M. D., Leontini, J. S., Thompson, M. C., Hourigan, K., 2011. Vortex shedding and three-dimensional behaviour of flow past a cylinder confined in a channel. Journal of Fluids and Structures 27 (5-6), 855–860.

Joly, A., Etienne, S., Pelletier, D., Jan. 2012. Galloping of square cylinders in cross-flow at low Reynolds numbers. Journal of Fluids and Structures 28, 232–243.

Leontini, J. S., Lo Jacono, D., Thompson, M. C., Nov. 2011. A numerical study of an inline oscillating cylinder in a free stream. Journal of Fluid Mechanics 688, 551–568.

Leontini, J. S., Thompson, M. C., 2013. Vortex-induced vibrations of a diamond cross-section: Sensitivity to corner sharpness. Journal of Fluids and Structures 39, 371–390.

Leontini, J. S., Thompson, M. C., Hourigan, K., Apr. 2007. Three-dimensional transition in the wake of a transversely oscillating cylinder. Journal of Fluid Mechanics 577, 79.

Lighthill, J., 1986. Fundamentals concerning wave loading on offshore structures. Journal of Fluid Mechanics 173, 667–681.

Luo, S., Chew, Y., Ng, Y., Aug. 2003. Hysteresis phenomenon in the galloping oscillation of a square cylinder. Journal of Fluids and Structures 18 (1), 103–118.

Ng, Y., Luo, S., Chew, Y., Jan. 2005. On using high-order polynomial curve fits in the quasi-steady theory for square-cylinder galloping. Journal of Fluids and Structures 20 (1), 141–146.

Païdoussis, M., Price, S., de Langre, E., 2010. Fluid-Structure Interactions : Cross-Flow-Induced Instabilities. Cambridge University Press.

Parkinson, G. V., Smith, J. D., 1964. The square prism as an aeroelastic non-linear oscillator. The Quarterly Journal of Mechanics and Applied Mathematics 17 (2), 225–239.

Sheard, G. J., Fitxgerald, M. J., Ryan, K., Jun. 2009. Cylinders with square cross-section: wake instabilities with incidence angle variation. Journal of Fluid Mechanics 630, 43.

Thompson, M., Hourigan, K., Sheridan, J., Feb. 1996. Three-dimensional instabilities in the wake of a circular cylinder. Experimental Thermal and Fluid Science 12 (2), 190–196.

Thompson, M. C., Hourigan, K., Cheung, A., Leweke, T., Nov. 2006. Hydrodynamics of a particle impact on a wall. Applied Mathematical Modelling 30 (11), 1356–1369.

Tong, X., Luo, S., Khoo, B., Oct. 2008. Transition phenomena in the wake of an inclined square cylinder. Journal of Fluids and Structures 24 (7), 994–1005.

Vio, G., Dimitriadis, G., Cooper, J., Oct. 2007. Bifurcation analysis and limit cycle oscillation amplitude prediction methods applied to the aeroelastic galloping problem. Journal of Fluids and Structures 23 (7), 983–1011.